IEEE Access
Multidisciplinary | Rapid Review | Open Access Journal

Received September 20, 2019, accepted October 7, 2019, date of publication October 17, 2019, date of current version October 30, 2019.

Digital Object Identifier 10.1109/ACCESS.2019.2948067

Denoising and Features Extraction of ECG Signals in State Space Using Unbiased FIR Smoothing

CARLOS LASTRE-DOMÍNGUEZ, (Member, IEEE), YURIY S. SHMALIY, (Fellow, IEEE), OSCAR IBARRA-MANZANO, (Member, IEEE), AND MIGUEL VAZQUEZ-OLGUIN, (Member, IEEE)
Department of Electronics Engineering, Universidad de Guanajuato, Salamanca 36885, Mexico

Corresponding author: Yuriy S. Shmaliy (shmaliy@ugto.mx)

This work was supported in part by the CONACyT under Grant A1-S-10287 (2017-2018) and in part by the PFCE 2019 awarded to the University of Guanajuato.

ABSTRACT The electrocardiogram (ECG) signals bear fundamental information for making decisions about different kinds of heart diseases. Therefore, many efforts were made during decades to extract features of heartbeats via ECG records with high accuracy and efficiency using different strategies and methods. In this paper, we solve the problem in discrete-time state-space using a novel q-lag unbiased finite impulse response (UFIR) smoother, which we adapt to the ECG signal shape via the time-varying optimal averaging horizon. It is shown that the adaptive UFIR smoother performs better in applications to ECG signals than the standard techniques such as the Savitsky-Golay, wavelet-based, low-pass, band-pass, notch, and median filters. Applications are given for the PhysioBank data benchmark, which contains several records taken from different databases such as the MIT-BIH Arrhythmia (MITDB). A complete statistical analysis is provided via normalized histograms and statistical classifiers. It is shown in a comparison with other methods that the adaptive UFIR smoother has a higher accuracy in denoising, features extraction, and features classification for ECG records with normal rhythm and atrial fibrillation (AF).

INDEX TERMS Biomedical signal processing, electrocardiogram (ECG) signal denoising, ECG features extraction, unbiased finite impulse response (UFIR) filtering.

I. INTRODUCTION

It is known that the electrocardiogram (ECG) signals bear essential information about different kinds of heart diseases. Therefore, different strategies have been developed during decades to investigate ECG signals and extract critical features with highest accuracy and efficiency [1]–[5]. Specifically, many algorithms have been designed to analyse and extract fiducial features and rhythm variabilities in ECG signals, noise detection based on agglomerative clustering of morphological features, and information extraction about the atrium behaviour. Morphological characteristics related to ECG signals are typically learned through the P, QRS, and T waves, using appropriate methods of ECG signal denoising and features extraction [5]–[16]. Even so, it is still challenging to reach accurate results due to measurement errors caused by data noise and artifacts induced by data acquisition equipment.

Methods developed for denoising and features extraction based on the Fourier transform assume that ECG signals are stationery and ignore time resolution. A better trade off between the frequency and time is guaranteed by the wavelet transform-based algorithms, provided that a proper wavelet is chosen [7], [17]–[30]. Other methods can also be applied to ECG signals, such as the empirical mode decomposition (EMD) and Hadamard transform [31], [32]. To increase the accuracy, several authors combined the above methods with approaches such as the principal component analysis (PCA) [33], [34], support vector machine (SVM) [35], and neural networks or deep learning techniques [30], [36].

In many cases, accurate features extraction of ECG signals requires more rigorous studies involving optimal methods mostly due to often unspecified noise attached to ECG data. In this regard, optimal smoothing is recognized as one of the most powerful techniques to remove noise while retaining fundamental properties of ECG signals. Specifically, the smoothing technique developed by Savitsky and Golay [37] is often applied to ECG signals [38]–[42]. A flaw is that the Savitsky-Golay smoother relates the estimates to the middle of the averaging horizon. As has been shown in [43], it provides suboptimal unbiased smoothing only for odd-degree polynomials, while for the even-degree

The associate editor coordinating the review of this manuscript and approving it for publication was Donato Impedovo.

polynomials an optimal lag q must be taken from other points. The theory of the p-shift, $q = -p > 0$, unbiased finite impulse response (UFIR) filtering, which considers the Savitsky-Golay smoother as a special case for odd-order polynomials, is given in [43] and developed in [44], [45]. To provide the best denoising effect, the approach suggests that an optimal lag q must be set individually for each polynomial and not obligatorily at the middle point. Furthermore, it provides smoothing filtering by $p < 0$, filtering by $p = 0$, and predictive filtering by $p > 0$. Let us also notice that the Savitsky-Golay filter was recently modified to be optimal in the minimum mean square error (MSE) sense [38], [40]. The modification is akin to the optimal UFIR filter [46], which produces a maximum likelihood estimate [47]. Because both these solutions require information about noise, which is not well studied in ECG signals, the use of the UFIR smoother becomes more preferable.

A disadvantage of the batch p-shift UFIR filter [43] resides in slow operation, which causes a computational burden and complexity in denoising and features extraction [48]. Moreover, the UFIR [43] and Savitsky-Golay [37] smoothers were designed to de-noise signal with no extra information about the ECG signal state required to facilitate features extraction. A more efficient state space iterative p-shift UFIR algorithm using recursions was designed by Shmaliy in [48] and then developed and applied with different purposes in many papers [43], [44]. Although the iterative UFIR smoother [48] provides much more information than the batch UFIR [43] and Savitsky-Golay [37] structures, its development for features extraction in ECG signals still has not been addresses in the literature that motivates our present work.

Referring to the first results obtained in [49], [50], where the batch UFIR smoothing filter has demonstrated a better performance than several other well-recognized estimators, in this paper we employ and develop an iterative UFIR smoother in state space. An objective is to increase accuracy of the features extraction and fiducial points detection.

The main contributions of the paper are the following:

- An optimal q-lag state-space UFIR smoothing algorithm for ECG signals denoising and artifacts removal.
- An algorithm for ECG signal stable features evaluation using different classifiers under the unknown noise.
- High-accuracy patterns classification for ECG signals with atrial fibrillation (AF) and normal conditions.

To reach the goal, we first provide denoising of ECG signals and compare the results obtained by the wavelet-based and some standard filters. We then extract features of the ECG-waves and analyse confidence intervals for particular ECG records. The results are tested by different classifiers and compared to others available from several machine learning techniques. The rest of the paper is organized as follows. Section II discusses the databases and signal model. Section III presents the discrete-time state-space UFIR filtering and smoothing approaches. In Section IV, we design an adaptive UFIR smoothing algorithm for ECG signal features extraction. Specifics of the UFIR smoother optimal tuning and testing are given in Section V. Applications to ECG signals are given in Section VI. Discussion of the results is provided in Section VII and conclusions are finally drawn in Section VIII.

II. ECG SIGNAL DATABASE AND MODEL

We base our investigation on the MIT-BIH Arrhythmia benchmark [51], which contains several records taken from different databases such as the MIT-BIH Arrhythmia (MITDB). The MITDB comprises 48 records with normal and abnormal rhythms taken from 47 subjects. The records are sampled to 360 Hz per lead with 11-bit resolution over a 10 mV range. This database provides the records in two leads, where the most common is the MLII (modified lead II). Other leads are also used, such as V1, V5, etc. A key issue is to choose the lead that most clearly reflects the ECG signal morphology.

A. MORPHOLOGICAL REPRESENTATION OF ECG SIGNAL FEATURES

A heartbeat or the ECG complex contains different waves divided among themselves by distinct intervals [52] (Fig. 1).

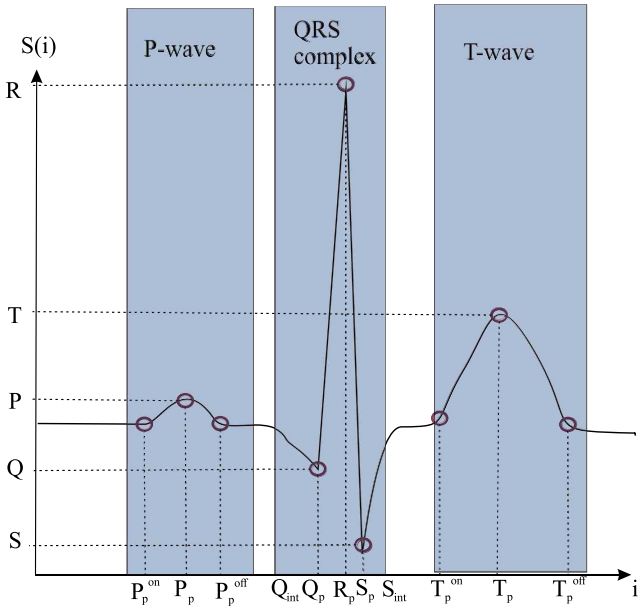

FIGURE 1. Features of a heartbeat pulse represented with fiducial points related with durations and amplitudes.

The P-wave represents a depolarization in the right and left atrial, which is provided by sinus node. Normally, the P-wave is positive in most of the leads. In LII (Lead II), the P-wave amplitude is registered to be larger [53]; it does not surpass 2, 5 mV and its duration does not exceed 0.1 s. The QRS complex follows by the P-wave and represents the ventricular depolarization. This complex is composed by Q, R and S points (sometimes called waves) and the duration of QRS complex normally ranges from 0.06 s to 0.10 s, although it varies with heartbeat rate (cardiac frequency) and is smaller

in children. The T-wave starts from the isophasic line and can adopt several forms such as tall, pointed, flattened, inverted and biphasic. The T wave length varies considerably. However, habitually it mostly measures 2 mm and is positive in all of the leads, excepts for aVR that is negative. The nature of the U-wave is still not well understood and it is hard to recognize this wave in most of the leads. What follows from many measurements is that this wave is positive.

B. ECG SIGNAL MODEL IN DISCRETE-TIME STATE-SPACE

To provide efficient denoising and features extractions, in this subsection we model an ECG signal in discrete-time state-space. We represent an ECG signal on a horizon $[m, n]$ of N points, from $m = n - N + 1$ to n, where n is the discrete time index, with a degree polynomial as shown in [50]. The inherent ECG noise is still not well understood and its incorrect description may cause estimation errors. Therefore, we suppose that the underlying process in each ECG pulse is time-invariant and deterministic. We also suppose that scalar measurements of the ECG signal are provided in the presence of zero mean noise having an unknown distribution (not obligatorily Gaussian) and covariance.

Under such assumptions, we represent an ECG signal in discrete-time state-space with the following state and observation equations, respectively,

$$\mathbf{x}_n = \mathbf{F}\mathbf{x}_{n-1}\,, \tag{1}$$

$$y_n = \mathbf{H}\mathbf{x}_n + v_n\,, \tag{2}$$

where $\mathbf{x}_n \in \mathbb{R}^K$ is the ECG process state vector, y_n is the scalar observation, v_n is the scalar measurement noise, $\mathbf{F} \in \mathbb{R}^{K\times K}$ is the system matrix projecting the initial state $\mathbf{x}_{n-1}$ to $\mathbf{x}_n$ and given by [54]

$$\mathbf{F} = \begin{bmatrix} 1 & \tau & \frac{\tau^2}{2} & \dots & \frac{\tau^{K-1}}{(K-1)!} \\ 0 & 1 & \tau & \dots & \frac{\tau^{K-2}}{(K-2)!} \\ 0 & 0 & 1 & \dots & \frac{\tau^{K-3}}{(K-3)!} \\ \vdots & \vdots & \vdots & \ddots & \vdots \\ 0 & 0 & 0 & \dots & 1 \end{bmatrix}. \tag{3}$$

For a scalar measurement, we assign the observation matrix as $\mathbf{H} = [\,1\,0\cdots 0\,] \in \mathbb{R}^{1\times K}$ and suppose that noise v_n is zero mean with unknown distribution and other statistics. The batch UFIR filter can now be applied to (1) and (2) to provide state estimates as in the following.

III. UFIR FILTERING AND SMOOTHING OF ECG SIGNALS

Provided modeling of an ECG signal in discrete-time state space, in this section we discuss the UFIR filter and smoother first in the batch form and then in a fast iterative form using recursions. Because the optimal averaging horizon is shape-varying for ECG signals, we also discuss its adaptive structure.

A. BATCH UFIR FILTER AND SMOOTHER

On a horizon $[m, n]$ of N ECG data points, the batch UFIR filtering estimate $\mathbf{x}_n \triangleq \hat{\mathbf{x}}_{n|n}$ of $\mathbf{x}_n$ is given by [48]

$$\hat{\mathbf{x}}_n = (\mathbf{W}_{m,n}^T\mathbf{W}_{m,n})^{-1}\mathbf{W}_{m,n}^T\mathbf{Y}_{m,n}\,, \tag{4}$$

where the extended observation vector $\mathbf{Y}_{m,n}$ and augmented measurement matrix $\mathbf{W}_{m,n}$ are, respectively,

$$\mathbf{Y}_{m,n} = [\,y_m^T\; y_{m+1}^T \cdots y_n^T\,]^T\,, \tag{5}$$

$$\mathbf{W}_{m,n} = \begin{bmatrix} \mathbf{H}(\mathbf{F}^{n-m})^{-1} \\ \vdots \\ \mathbf{H}\mathbf{F}^{-1} \\ \mathbf{H} \end{bmatrix}. \tag{6}$$

In the discrete convolution-based form, estimate (4) can be represented as

$$\hat{\mathbf{x}}_n = \mathcal{H}_{m,n}\mathbf{Y}_{m,n}\,, \tag{7}$$

where the UFIR filter gain matrix $\mathcal{H}_{m,n}$ given by

$$\mathcal{H}_{m,n} = (\mathbf{W}_{m,n}^T\mathbf{W}_{m,n})^{-1}\mathbf{W}_{m,n}^T \tag{8}$$

can be rewritten as

$$\mathcal{H}_{m,n} = \mathbf{G}_n\mathbf{W}_{m,n}^T\,, \tag{9}$$

where $\mathbf{G}_n$ is the generalized noise power gain (GNPG),

$$\mathbf{G}_n = \mathcal{H}_{m,n}\mathcal{H}_{m,n}^T = (\mathbf{W}_{m,n}^T\mathbf{W}_{m,n})^{-1}\,. \tag{10}$$

Given the UFIR filtering estimate $\hat{\mathbf{x}}_n \triangleq \hat{\mathbf{x}}_{n|n}$ of $\mathbf{x}_n$ by (7), the q-lag UFIR smoothing estimate can be obtained by projecting $\hat{\mathbf{x}}_n$ into $\hat{\mathbf{x}}_{n-q}$ as shown in [43],

$$\hat{\mathbf{x}}_{n-q|n} = \mathbf{F}^{-q}\hat{\mathbf{x}}_{n|n}\,, \tag{11}$$

where $q_{\text{opt}} = \lfloor \frac{N}{2} \rfloor$ is a digital optimal lag for odd-degree UFIR smoothers and q_{opt} must be set individually following Fig. 8 in [43] for each even-degree. Let us notice again that the Savitsky-Golay solution ignores this specific and suggests taking lags from the middle points of $[m, n]$ for all degrees that introduces errors.

B. ADAPTED OPTIMAL HORIZON N_{apt}

Of importance is that the UFIR filter is able to minimize the MSE on $[m, n]$, if the horizon N is set optimally as N_{opt} [55]. To make it possible in the absence of the reference signal (ground truth), we follow [55] and find N_{opt} for ECG signals by minimizing the trace of the derivative of the mean square value (MSV) of the measurement residual matrix $\mathbf{V}(N)$ as

$$\hat{N}_{\text{opt}} = \arg\min_N \frac{\partial\,\text{tr}\,\mathbf{V}(N)}{\partial N} + 1\,. \tag{12}$$

A solution to the optimization problem (12) has been provided in our early paper together with an algorithm [50], which we will further use. It has been found out in [50] that an optimal horizon $N_{\text{opt}} = 21$ serves for the 2-degree polynomial corresponding to three states, $K = 3$, and database [51] exploited in this paper.

An important specific is that N_{opt} varies on different parts of the ECG signals [49]. Therefore, we will make N_{opt} adaptive (N_{apt}) to range from $N_{\min} = K = 3$ to N_{opt} as

$$N_{\min} \leqslant N_{\text{apt}} \leqslant N_{\text{opt}}\,,$$

where $N_{\min}$ is a minimum horizon applied to a fast excursion between Q_{p} and S_{p} (Fig. 1). To this end, we recognize five parts in the ECG signal separated with the following points in Fig. 1: Q_{int}, Q_{p}, S_{p}, and S_{int}. Up to Q_{int}, a smooth part of the ECG signal is processed with N_{opt}. Between Q_{int} and Q_{p}, the horizon N_{apt} linearly reduces from N_{opt} to $N_{\min}$. The QRS complex, between Q_{p} and S_{p}, is processed with $N_{\min}$ to follow exactly a fast excursion around R_{p}. From S_{p} to S_{int}, the horizon N_{apt} linearly increases from $N_{\min}$ to N_{opt}, The horizon finally becomes N_{opt} above S_{int}. Accordingly, adaptive UFIR smoothing is provided as

$$\hat{\mathbf{x}}_{n-q|n} = \begin{cases} \hat{\mathbf{x}}_{n-q|n}(N_{\text{opt}})\,, & 1 \leqslant n \leqslant \text{Q}_{\text{int}} - 1\,, \\ \hat{\mathbf{x}}_{n-q|n}(N_{\text{apt}})\,, & \text{Q}_{\text{int}} \leqslant n \leqslant \text{Q}_{\text{p}} - 1\,, \\ \hat{\mathbf{x}}_{n-q|n}(N_{\min})\,, & \text{Q}_{\text{p}} \leqslant n \leqslant \text{S}_{\text{p}}\,, \\ \hat{\mathbf{x}}_{n-q|n}(N_{\text{apt}})\,, & \text{S}_{\text{p}} + 1 \leqslant n \leqslant \text{S}_{\text{int}}\,, \\ \hat{\mathbf{x}}_{n-q|n}(N_{\text{opt}})\,, & \text{S}_{\text{int}} + 1 \leqslant n \leqslant T\,, \end{cases} \tag{13}$$

where T represents the heartbeat length. Provided N_{apt}, we can next design an iterative UFIR smoothing algorithm using recursions, which reduces the computational load.

C. ITERATIVE UFIR SMOOTHING

Like the Kalman filter (KF), iterative computation of the batch UFIR estimate (7) is provided recursively in two phases: *predict* and *update* [48]. In contrast to the KF, the UFIR algorithm does it with no requirements for the noise statistics and initial values and is thus more suitable for ECG signals in view of generally unknown heartbeat noise.

At the predict phase, the UFIR algorithm computes the prior state estimate $\hat{\mathbf{x}}_n^- = \mathbf{F}\hat{\mathbf{x}}_{n-1}$ and ignores the prior error covariance, unlike the KF. At the update phase, the UFIR algorithm updates the GNPG $\mathbf{G}_n$ as $\mathbf{G}_n = [\mathbf{H}^T\mathbf{H} + (\mathbf{F}\mathbf{G}_{n-1}\mathbf{F}^T)^{-1}]^{-1}$, the measurement residual $z_n = y_n - \mathbf{H}\hat{\mathbf{x}}_n^-$, the bias correction gain $\mathbf{K}_n = \mathbf{G}_n\mathbf{H}^T$, and the state estimate $\hat{\mathbf{x}}_n = \hat{\mathbf{x}}_n^- + \mathbf{K}_n z_n$. A pseudo code of the UFIR smoothing algorithm [48] adapted to ECG signals is listed as Algorithm 1.

Provided ECG data y_n, adaptive horizon N_{apt}, and optimal lag q_{opt} for a chosen filter degree, Algorithm 1 starts self-computing the initial GNPG G_s and initial state $\tilde{\mathbf{x}}_s$ at s, which corresponds to a short initial horizon of K points. This is required to overcome singularities in the UFIR filter gain on shorter horizons. Estimate $\hat{\mathbf{x}}_n$ at time index n is computed iteratively, using an auxiliary time variable l, which starts with $l = n - N_{\text{apt}} + K + 1$ and finishes when $l = n$. The estimate $\hat{\mathbf{x}}_n$ obtained in such a way minimizes the MSE and is called the optimal UFIR estimate. Provided $\hat{\mathbf{x}}_n$, the UFIR smoothing estimate with a lag q is obtained by a projection from n to $n - q$ as [48]

$$\hat{\mathbf{x}}_{n-q} = \mathbf{F}^{-q}\hat{\mathbf{x}}_n \tag{14}$$

Algorithm 1 Adaptive Iterative UFIR Smoothing Algorithm for ECG Signals

Data: y_n, $N = N_{\text{apt}}$, $q = q_{\text{opt}}$
Result: $\hat{\mathbf{x}}$

Begin:
for $n = N - 1, N, \ldots$ **do**
  $m = n - N + 1$, $s = n - N + K$
  $\mathbf{G}_s = (\mathbf{W}_{m,s}^T\mathbf{W}_{m,s})^{-1}$
  $\tilde{\mathbf{x}}_s = \mathbf{G}_s\mathbf{W}_{m,s}^T\mathbf{Y}_{m,s}$
  for $l = s + 1$ to n **do**
    $\tilde{\mathbf{x}}_l^- = \mathbf{F}\tilde{\mathbf{x}}_{l-1}$
    $\mathbf{G}_l = [\mathbf{H}^T\mathbf{H} + (\mathbf{F}\mathbf{G}_{l-1}\mathbf{F}^T)^{-1}]^{-1}$
    $\mathbf{K}_l = \mathbf{G}_l\mathbf{H}^T$
    $\tilde{\mathbf{x}}_l = \tilde{\mathbf{x}}_l^- + \mathbf{K}_l(y_l - \mathbf{H}\tilde{\mathbf{x}}_l^-)$
  end for
  $\hat{\mathbf{x}}_n = \tilde{\mathbf{x}}_n$
  $\hat{\mathbf{x}}_{n-q} = \mathbf{F}^{-q}\hat{\mathbf{x}}_n$
end for

and we notice again that lag q must be set optimally as q_{opt} to reach minimum possible smoothing errors.

IV. ECG SIGNAL FEATURES EXTRACTION IN STATE SPACE

Features extraction from ECG signals in state space using Algorithm III-C is provided in five stages (Fig. 2): 1) detrending, 2) QRS-complex detection, 3) segmentation, 4) adaptive iterative UFIR smoothing, and 5) windowing of ECG waves.

1) DETRENDING

At this state, Algorithm III-C is applied on a large horizon $N \gg N_{\text{opt}}$ to remove artifacts from the external systems.

2) QRS-COMPLEX DETECTION

The QRS-complex is detected using annotations of the arrhythmia MIT-BIH database following the approach proposed by Tompkins and Pan and Tompkins [56]. Note that a majority of annotations detect the QRS complex with a probability of 99.3%.

3) SEGMENTATION

Localized the QRS-complex, a closest point to the R-peak is detected in each heartbeat. Next, by taking 100 samples to the left and 200 samples to the right, a window is created to outline a heartbeat as in Fig. 1. If this window does not cover all points of interest (P-wave, QRS-complex, and T wave), its width is increased. The segmentation process is organized heuristically with the aim of analysing the morphological waves. We refer to this technique described in [57]–[59].

4) ITERATIVE UFIR SMOOTHING

Specified N_{opt} and N_{apt} for the database used as shown in [50], the horizon $N_{\text{opt}} = 21$ is applied beyond the QRS complex. To avoid large bias errors, N_{apt} specified by (13) is applied over all EGC signal. Provided UFIR filtering, smoothing with a lag q is organized using (14).

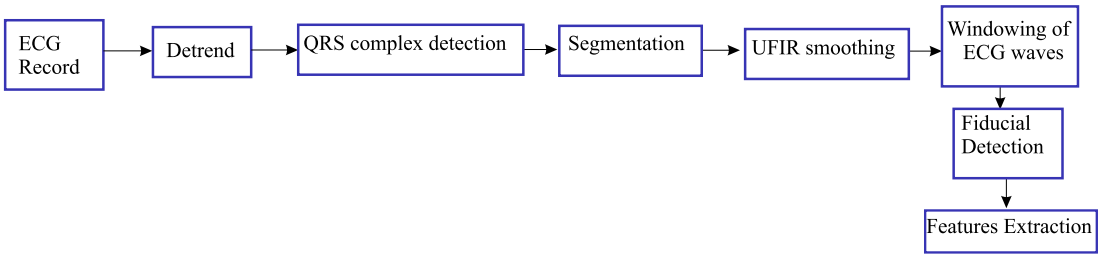

FIGURE 2. Block-diagram of features extraction of the ECG signal in state space using an UFIR smoother.

5) WINDOWING OF ECG WAVES

The UFIR smoother provides denoising and estimation of the ECG signal three states as shown in Fig. 3 for the first state (de-noised ECG signal), second state (time derivative of the de-noised signal), and third state (second time derivative of the de-noised signal). Using information about the ECG signal states, the R-peak, QRS_{max}, and QRS_{min} are determined and a window is applied to cover the QRS complex. The P-waves detection is provided beginning from Q until the heartbeat ends. Here, a window is applied to cover P_{on}, P-peak, P_{off} points, which are determined by P_{max} and P_{min} in the second state. Similarly, the T-wave is detected, in which case T_{on} and T_{off} are covered by a window created for T_{max} and T_{min} (Fig. 3b).

A. FIDUCIAL POINTS DETECTION AND FEATURES EXTRACTION

In this section, we use the above results to provide fiducial points detection and features extraction, such as the durations and amplitudes of different detected fiducial points. Provided windowing of the P-wave, QRS-complex, and T-wave, we use the fiducial point P_{on} as an initial point of P-wave, P as a P-peak, P_{off} as a final point of P-wave, Q as an initial point of QRS complex, R as a R-peak, S as a final point of QRS complex, T_{on} as a initial point of T-wave, T as T-peak, and T_{off} as a final of T-wave. The fiducial points are extracted as follows.

1) QRS-COMPLEX

The fiducial points for a QRS-complex are determined by finding a maximum QRSmax and a minimum QRSmin in the second state (Fig. 4b), which are corroborated by the third state at zero cross points (Fig. 4c). Two variables "dqrs1" and "dqrs2" are introduced to calculate the initial and final points of a QRS-compex. The R-peak is detected as $\hat{R}$ at a zero cross point of the second state and is corroborated by QRSmin of the third state.

2) P AND T WAVES

The fiducial points for P and T waves are determined by finding Pmax, Tmax, Pmin, and Tmin in the second state (Fig. 3b), which are corroborated by the third state at zero cross points (Fig. 3c). Two variables "dp1" and "dp2" are introduced to calculate the initial and final points of the P-wave. Similarly, two variables "dt1" and "dt2" are introduced for the T-wave. The P-peak and T-peak assigned as $\hat{P}$ and $\hat{T}$, respectively, are detected at the zeros cross of the second state. These points are confirmed by Pmin and Tmin in Fig. 3.

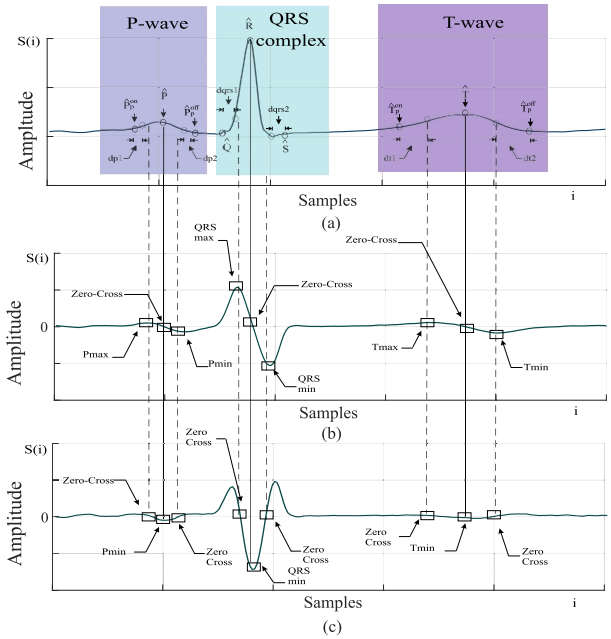

FIGURE 3. Fiducial features of a single heartbeat extracted along with the spacial points in state space using the UFIR approach: (a) first state, (b) second state, and (c) third state.

Provided the fiducial points $\hat{P}_p^{on}$, $\hat{P}$, $\hat{P}_p^{off}$, $\hat{Q}$, $\hat{R}$, $\hat{T}_p^{on}$, $\hat{T}$, $\hat{T}_p^{off}$ to represent the relevant points[1] in Fig. 1, the ECG wave durations and amplitudes are calculated for the P-wave as

$$P_{dur} = P_p^{off} - P_p^{on} \cong \hat{P}_p^{off} - S\hat{P}_p^{on}, \tag{15}$$

$$P_{amp} = S(P_p) - S(P_p^{on}) \cong \hat{P} - S(\hat{P}_p^{on}), \tag{16}$$

for the QRS-complex as

$$QRS_{dur} = S_p - Q_p \cong \hat{S}_p - \hat{Q}_p, \tag{17}$$

$$QRS_{amp} = R - S(Q_p) \cong \hat{R} - S(\hat{Q}_p), \tag{18}$$

[1]The points P_p, Q_p, R_p, S_p and T_p are time indexes that determine the peaks P-peak, Q-point, R-peak, S-point and T-peak in the heartbeat.

and for the T-wave by

$$\mathrm{T_{dur}} = \mathrm{T_p^{off}} - \mathrm{T_p^{on}} \cong \hat{\mathrm{T}}_\mathrm{p}^{\mathrm{off}} - \hat{\mathrm{T}}_\mathrm{p}^{\mathrm{on}}, \tag{19}$$

$$\mathrm{T_{amp}} = \mathrm{S(T_p)} - \mathrm{S(T_p^{on})} \cong \hat{\mathrm{T}} - \mathrm{S}(\hat{\mathrm{T}}_\mathrm{p}^{\mathrm{on}}). \tag{20}$$

Note that estimates $\hat{\mathrm{P}}_\mathrm{p}^{\mathrm{on}}$, $\hat{\mathrm{P}}_\mathrm{p}^{\mathrm{off}}$, $\mathrm{S}(\hat{\mathrm{Q}}_\mathrm{p})$, $\hat{\mathrm{T}}_\mathrm{p}^{\mathrm{on}}$, and $\hat{\mathrm{T}}_\mathrm{p}^{\mathrm{off}}$ represent points, which belong to the base line of an ECG signal.

V. TUNING AND TESTING

In order to achieve the best smoothing effect, in this section we tune the UFIR smoother to the ECG signals in terms of optimal lags related to optimal horizons. As benchmarks, we will employ the wavelet-based, low-pass, high-pass, median, and notch filters employed in [8], [28], [60]–[63].

A. OPTIMAL LAG FOR UFIR SMOOTHER

It has been shown in [43] that an optimal lag q_{opt} for odd-order polynomial UFIR smoothers must be taken from the middle of an optimal averaging horizon of N_{opt} points. Accordingly, we specify q_{opt} as

$$q_{\mathrm{opt}} = \left\lfloor \frac{N_{\mathrm{opt}} - 1}{2} \right\rfloor, \tag{21}$$

where $\lfloor x \rfloor$ means the floor of x, i.e. the largest integer less than or equal to x.

For even-order polynomials, [43] suggests that q_{opt} must be set individually. For the second-order UFIR smoother we thus follow [43] and set

$$q_{\mathrm{opt}} = \frac{N_{\mathrm{opt}} - 1}{2} - \frac{1}{2}\sqrt{\frac{N_{\mathrm{opt}}^2 + 1}{5}}. \tag{22}$$

In this regard, let us notice that even though the Savitsky-Golay smoother [37] was derived from different prospectives, it has a similar structure with the UFIR smoother and similar properties such as adaptability to signal variations and robustness to noise. An advantage of the UFIR approach is that it suggests optimal lag for each smoother degree [43] that was not provided by Savitsky and Golay.

B. TESTING THE ITERATIVE UFIR ALGORITHM

The three-state polynomial model was shown in [50] to be near optimal for ECG signals. Referring to [50], we represent the system and measurement matrices as, respectively,

$$\mathbf{F} = \begin{bmatrix} 1 & \tau & \frac{\tau^2}{2} \\ 0 & 1 & \tau \\ 0 & 0 & 1 \end{bmatrix}, \quad \mathbf{H} = [\,1\ 0\ 0\,], \tag{23}$$

where a discrete time-step $\tau = 1/f$ is due to the sampling frequency of $f = 360$ Hz used in DataBase MIT-BIH Arrhythmia. For (23), the augmented measurement matrix becomes

$$\mathbf{W}_{m,n} = \begin{bmatrix} \mathbf{H}\mathbf{F}^{-2} \\ \mathbf{H}\mathbf{F}^{-1} \\ \mathbf{H} \end{bmatrix}. \tag{24}$$

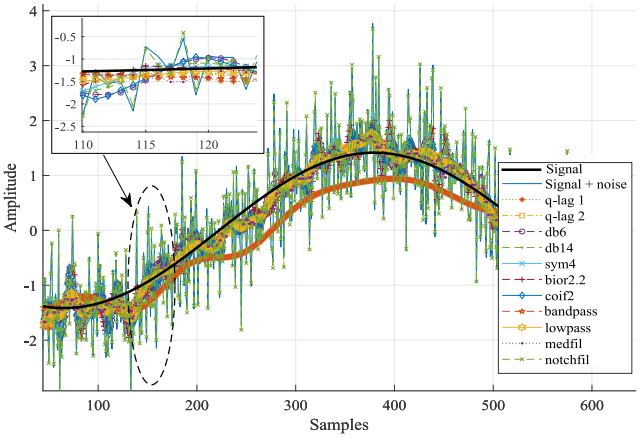

FIGURE 4. Denoising of a test sinusoid signal (solid) corrupted by zero mean AWGN using the UFIR smoother (dotted with asterisk) with lag q1 (21) and (dash-dotted and marked square) with lag q2 (22). The Daubechies wavelet-based smoothers are: db6 (dashed with marked circle), db14 (dash with dot marked), sym4 (solid with marked cross), bior2.2 (dashed with marked plus sing), coif2 (solid with marked diamond). The standard filters are: band pass filter (bandpass, dashed with marked pentagon), low pass filter low-pass (solid with marked hexagon), median (medfilt, dotted with marked point), and notch (notchfil, dashed with marked point).

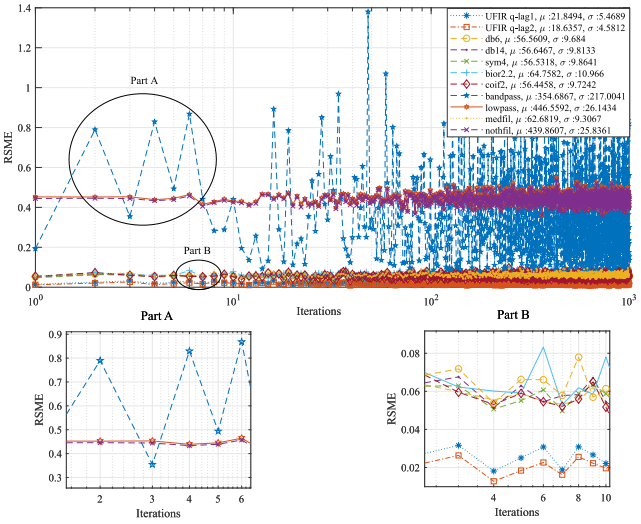

FIGURE 5. RMSEs corresponding to Fig. 4 and computed over 1000 iterations for the UFIR smoother, wavelet-based, and standard filters such as the low-pass, band-pass, median, and notch.

At these stage, we compare performances of the UFIR smoother relying on q_{opt} (21) and (21) and several other available filters. To test estimators, we generate a signal $s(n) = \sin(n)$ corrupted by an additive zero mean white Gaussian noise (WGN) having the variance $\sigma^2 = 0.0625$ and sketch the results in Fig. 4.

As can be seen, the UFIR smoother with q_{opt} (22) is most successful in accuracy, since its estimate ranges most close to the generated signal.

The root mean square errors (RMSEs) corresponding to Fig. 4 and computed over 1000 iterations and are shown in Fig. 5.

One observes that all wavelet-based and standard filters produce much larger errors than the UFIR smoothers

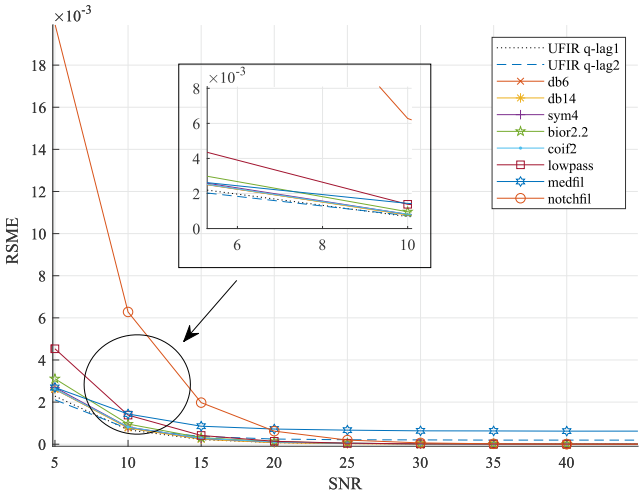

FIGURE 6. RMSEs of the UFIR smoother compared to the wavelets-based and standard filters.

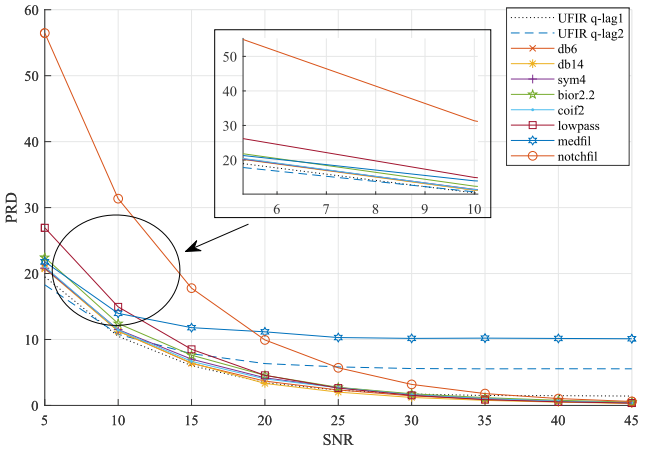

FIGURE 7. Smoothing errors in terms of PRD produced by diverse filters.

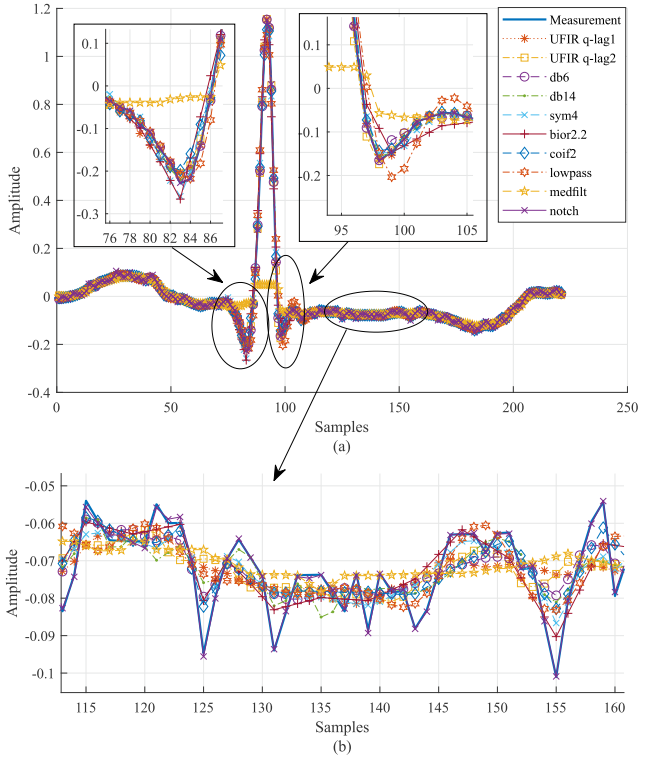

FIGURE 8. ECG signal denoising: (a) heartbeat estimation with the UFIR smother, wavelet-based filters, and standard filters; (b) segmental visualization of ten estimates.

irrespective of the wavelet chosen. Among the two UFIR smoothers used, the second one performs better due to the optimal lag (22). This simulation confirms the fact that the lag must be chosen optimally for all even-order smoothers, unlike for the Savitsky-Golay filter.

We next provide an analysis of the signal-to-noise ratios (SNRs) at the filter outputs in terms of the percentage root mean square (PRD). In doing so, a synthetic ECG signal is considered with known ECG signal and noise. The pass-band filter is set aside due to the instability (Fig 5). As can be seen in Fig. 6, both UFIR smoothers (q-lag1 and q-lg2) are most successful in accuracy for small and large SNR values. The notch filter produce considerable errors when the SNR drops below 10 dB. The wavelet-based smoothers perform well when the SNR exceed 20 dB and the low-pass filter performs similarly. It is also seen that the median filter is less accurate among other solutions when the SNR exceeds 20 dB.

Another experiment has been conducted to analyse the error variability with respect to the signal energy. The results are sketched in Fig. 7 in terms of the PRD. Again we notice that both UFIR smoothers produce smallest errors among other solutions.

VI. APPLICATIONS

In this section, we make efforts to extract features of ECG signals with a highest available accuracy provided by the adaptive UFIR smoothing algorithm designed based on the MIT-BIH Arrhythmia benchmark [51], which contains several records taken from different databases such as the MIT-BIH Arrhythmia (MITDB). The wavelet-based filters with several Daubechies mother wavelets will be used as benchmarks.

A. FILTERING AND ARTIFACT REMOVAL

What we expect from the estimates of the first state is that the outputs of the UFIR smoother with lags (21) and (22) and the outputs of the wavelet-based filters will not get away significantly from one another. Herewith, we suppose that errors in the estimates of the second and third states provided by the Savitsky-Golay smoother and wavelet-based filters will range higher than in the UFIR smoother, because the former estimates the high-order states via the derivatives, while the later makes it in state space concurrently. Our expectations are confirmed in Fig. 8, where we also highlight a part with clearly seen bias errors when an ECG signal changes rapidly within the QRS-complex.

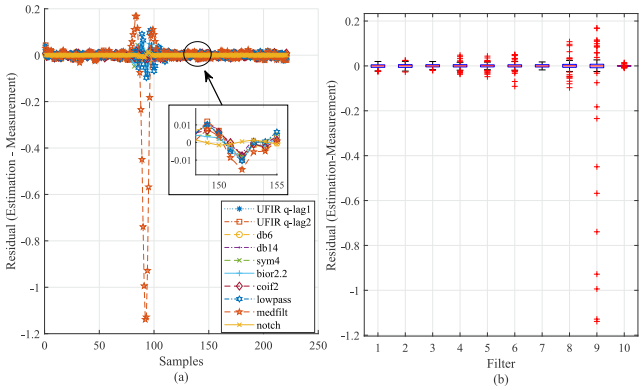

FIGURE 9. Measurement residuals produced by the UFIR smoother (q-lag1 and q-lag2), wavelet-based filters (db6, db14, sym4, bior2.2, and coif2), low-pass filter, median filter, and notch filter: (a) actual residuals and (b) error boxplot of heartbeat.

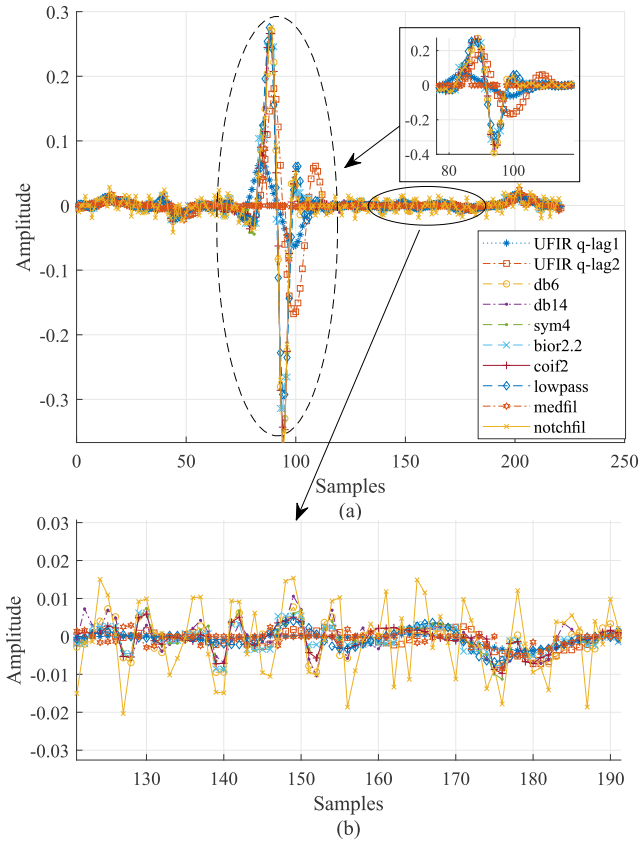

FIGURE 10. Estimates of the second state (first time-derivative) provided by the Savitsky-Golay smoother with lag q1 (21), UFIR smoother with lag q2, wavelet-based filters (db6, db14, sym4, bior2.2, and coif2), low-pass filter, median filter, and notch filter.

To sketch a more clear error picture, in Fig. 9 we give the measurement residuals produced by different estimators. What follows from this figure is that the UFIR smoother outperforms the wavelet-based and standard filters over all data, especially within the QRS complex. In Fig. 10, we give estimates of the second state provided by the estimators within

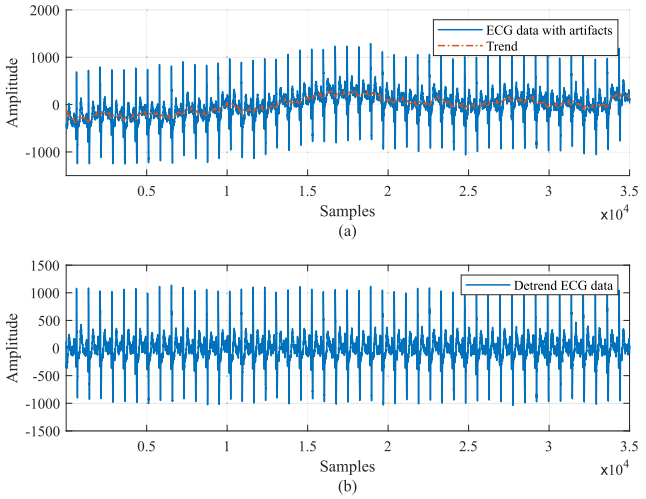

FIGURE 11. Baseline removal using UFIR smoothing with N = 1001 and *q*-lag2.

and beyond the QRS-complex. This figure also confirms that the UFIR smoother is most accurate among other solutions.

An important specific is that the UFIR smoother is able to remove efficiently artifacts as shown in Fig. 11. This property is useful to detrend the process, such as that shown in Fig. 2.

B. COMPUTATIONAL COMPLEXITY

Although the computation time is not strictly limited in ECG signals processing, an issue may arise when the consumed time is unacceptably large for medical needs. To find out how fast each algorithm operates under the same conditions, we next process an ECG record of 30 seconds with 1000 iterations. We base the computation time measurement on the MATLAB R2019 operating on a computer with intel core i7-4510U CPU (2.60) GHz and 16.0 GB RAM. The consumed times are listed in Table 1 and it is seen that an increase in the accuracy in the UFIR smoother is achieved at expense of the computation time, which is largest among other solutions, because the UFIR algorithm III-C has the $\mathcal{O}(N)$ complexity [48]. Even so, the time consumed by the UFIR smoother can be acceptable for medical needs, provided that the result demonstrates the highest accuracy. Note that the UFIR algorithm still was not optimized in terms of fast operation and the computation time can be significantly reduced in special implementations.

C. FEATURES EXTRACTION AND ERRORS COMPARISON

Provided estimates of the ECG signal states, we next conduct accurate features extraction following the above discusses scheme, in which relations (19) and (20) are used to extract features of the P-wave, (21) and (22) to compute the QRS-complex duration and amplitude, and (23) and (24) to extract features of the T-wave.

An extraction of the P-wave duration using the UFIR smoother is illustrated in Fig.12, where we also sketch estimates provided by some wavelet-based filters. The estimates

TABLE 1. Computation time required by diverse algorithms.

Algorithm	Average time (sec)	Parameter
UFIR q-lag 1	6.81	N=21
UFIR q-lag 2	5.48	N=21
db6	0.1610	level=3
db14	0.1521	level=3
sym4	0.1424	level=3
bior 2.2	0.1379	level=3
Coif2	0.1331	level=3
lowpass	0.3556	30Hz
medfilt	0.0029	–
notchfil	0.0015	60Hz

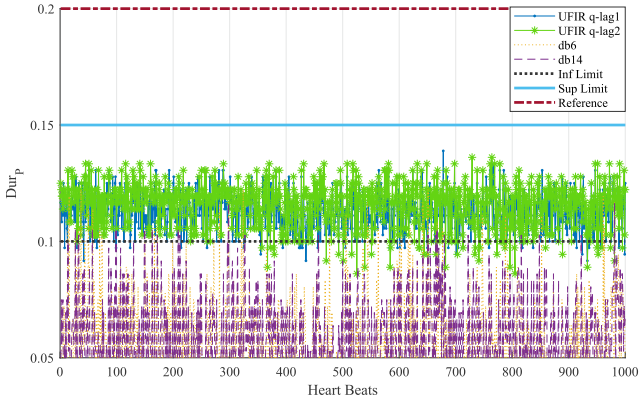

FIGURE 12. Extracted features of the P-wave duration Dur_P. Expert annotations (gold standard) [52] are represented with the upper and lower boundaries (solid lines) along with an expected average.

are given along with the expert annotations (gold standard) taken from [52], [57], [64] and shown as the upper and lower boundaries corresponding to the confidence interval of the probability of 95%.

Several features extracted using the UFIR smoother and other algorithms are generalized in Fig. 13. Again we see that the UFIR smoother provides estimates consistent with the gold standard, while the wavelet-based and standard filters are not always successful and their estimates undergo hight variabilities leading to inconsistent outputs. A more deep investigation respect to the P-wave will be provided next for normal and abnormal ECG signals.

D. APPLICATIONS TO NORMAL AND ABNORMAL ECGs

As an example of applications, we now extract features of the P-wave related to records with normal rhythm and atrial fibrillation and illustrate the results obtained using the wavelet filter with Db6 (Fig. 14) and UFIR smoother (Fig. 15).

The following observations follow from an analysis of these figures:

- The UFIR smoother puts the extracted features within the confidence interval that allows getting a strong discrimination between the normal and abnormal records as will be shown latter.
- All other algorithms produce unstable estimates (Fig. 13), which range out of the gold standard boundaries. Thus, making a good determination between the normal and abnormal records is more problematic by these filters.

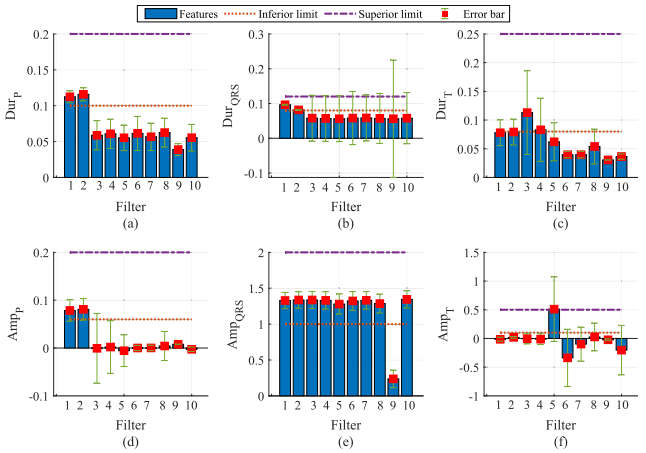

FIGURE 13. Features extracted using the UFIR smoother with *q*-lag1 (filter 1) and *q*-lag2 (filter 2) and other algorithms depicted as db6 (filter 3), db14 (filter 4), sym4 (filter 5), bior2.2 (filter 6), coif2 (filter 7), low-pass (filter 8), median (filter 9), and notch (filter 10): (a) duration Dur_P of P-wave, (b), duration Dur_{QRS} of QRS-complex, (c), duration Dur_T of T-wave, (d), amplitude Amp_P of P-wave, (e) amplitude Amp_{QRS} of QRS-complex, and (f) amplitude Amp_T of T-wave. Features are extracted from record 100 lead II of arrhythmia MIT-BIH database.

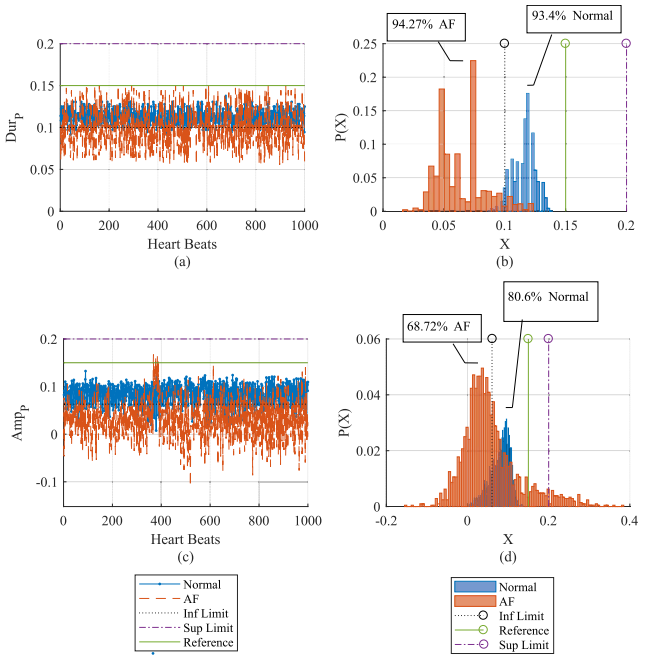

FIGURE 14. Features of the P-wave duration extracted using the wavelet-based filter with db6 from the AF and Normal ECG of MIT-BIH Arrhythmia Database: (a) Dur_P, (b) Dur_P normalized histogram, (c) Amp_P, and (d) Amp_P normalized histogram.

E. CLASSIFICATION

We now evaluate features provided by (15), (16), (17), (18), (19) and (20) using nine classifiers. Considering 29266 heartbeats including healthy and abnormal heartbeats, we first train the classifiers by the cross-validation process 10

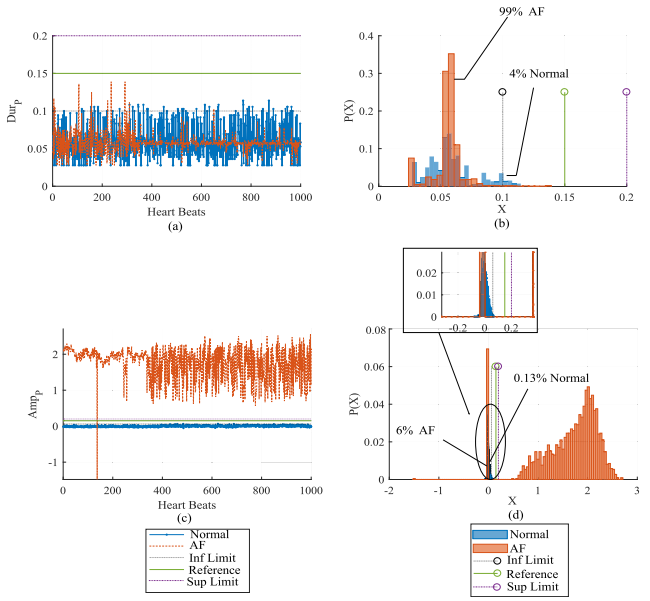

FIGURE 15. Features of the P-wave duration extracted using the UFIR smoother from the AF and Normal ECG of MIT-BIH Arrhythmia Database: (a) Dur_P, (b) Dur_P normalized histogram, (c) Amp_P, and (d) Amp_P normalized histogram.

considering records 100, 103, 105, 201, 203, 210 from arrhythmia MITDB. Next, the classifiers are tested by new data 106, 112,113, 219, 221 taken from arrhythmia MITDB. All data are divided into several balanced sets to avoid biases produced by imbalanced data (a specific class set is larger than other). The metrics used for performance assessment are accuracy (Acc.), specificity (Spec.), and sensitivity (Sens.),

$$\text{Acc} = \frac{\text{TP}+\text{TN}}{\text{TP}+\text{TN}+\text{FP}+\text{FN}}, \tag{25}$$

$$\text{Spec} = \frac{\text{TN}}{\text{TP}+\text{FN}}, \tag{26}$$

$$\text{Sens} = \frac{\text{TP}}{\text{TN}+\text{FP}}, \tag{27}$$

where, TP (true positives) means that healthy heartbeats are correctly classified, TN (true negatives) means that abnormal heartbeats are correctly classified, FN (false negatives) means that healthy heartbeats are classified as abnormal heartbeats, and FP (false positives) means that abnormal heartbeats are classified as healthy heartbeats.

By these metrics, the performance of each classifier turns out to be averaged that is seen in Table 2 representing the general classifier performance provided by the tree model (complex tree, medium tree, and simple tree), logistic regression, ensemble model (bagged tree, support vector machine (SVM) (linear, quadratic, and cubic), and subspace k-nearest neighbour (KNN). Note that the best classifiers were selected during the initial training. A similar process was organized by applying the principal component analysis (PCA) (See Table 3) and comparing the effects. It follows from both cases that the UFIR smoothing approach provides a considerably better performances that follows from Table 4, where a

TABLE 2. Performance of the AF for normal ECG heartbeats based on different classifiers.

Classifier	Acc.	Spec.	Sens.
Complex Tree	0.9664	0.9710	0.9964
Medium Tree	0.9664	0.9710	0.9964
Simple Tree	0.9664	0.9614	0.9952
Logistic Regression	0.9160	0.9814	0.9611
Bagged Tree	0.9934	0.9996	0.9855
Linear SVM	0.9275	0.9889	0.8827
Quadratic SVM	0.8331	0.9889	0.7604
Cubic SVM	0.8072	0.8949	0.7887
Subspace KNN	0.8072	0.9823	0.5988

TABLE 3. Performance of the AF and normal ECG signals applying PCA and based on different classifiers: FG SVM is the fine gaussian SVM, CG SVM is the coarse gaussian SVM.

Classifier	Acc.	Spec.	Sens.
Complex Tree	0.7144	0.7973	0.6221
Medium Tree	0.6942	0.7201	0.6655
Simple Tree	0.6757	0.5575	0.8073
Logistic Regression	0.8410	0.7514	0.9043
Linear SVM	0.8244	0.7527	0.7441
Quadratic SVM	0.8272	0.9019	0.4940
FG SVM	0.7804	0.8526	0.7848
CG SVM	0.7887	0.7560	0.6957
Bagged Tree	0.7801	0.8126	0.8474

TABLE 4. Comparative study of AF detection using different approaches and the UFIR smoother (UFIRS).

Studies	Acc	Sens.	Spec.	Approach
Maji *et al.* [32]	–	96.0%	–	EMD
Padmavathi *et al.* [9]	100%	–	–	AR
Lee *et al.* [31]	99.5%	99.9%	98.7%	HT
Annavarapu *et al.* [10]	–	97.2%	95.9%	RR-interval
Runnan He *et al.* [30]	99.2%	99.41%	98.9%	WT + CNN
Tateno *et al.* [11]	–	91.20%	96.08%	RR-interval
Alcaraz *et al.* [8]	88.84%	–	–	notch filter
Proposed method	99.3%	99.6%	99.9%	UFIRS

comparison is provided using the empirical mode decomposition (EMD), autoregressive model (AR), Hadamard transform (HT), wavelet transform (WT), and convolutional neural networks (CNN).

VII. DISCUSSION

The purpose of this investigation was to remove the measurement noise and extract concurrently features of ECG signals in state space using the q-lag UFIR smoother. This smoother does not require the noise statistics and initial values and is thus more suitable for ECG signals, whose noise is still not well understood. We were focused on the morphological features of individual ECG signals with normal rhythm and atrial fibrillation. To reach the highest accuracy allowed by the UFIR smoothing approach, we have developed an efficient algorithm and tested it by diverse ECG data in a comparison with other available techniques. The test has confirmed our expectations. Namely, the UFIR smoother considerably outperformed several standard algorithms in noise reduction and accuracy. That has become possible by setting optimal lags and adaptive horizons to the UFIR smoothing algorithm.

As benchmarks, we employed several wavelet-based filters and standard filters such as the low-pass, pass-band, median, and notch. A comparative analysis has shown that the UFIR smoother extracts the ECG signal specific features with higher accuracy than other solutions. That was also expected, since the wavelet-based algorithms do not allow for time-varying dynamic optimization similar to the adaptive UFIR structures, at least we did not find relevant solutions suggested for ECG signals in the wavelet area. A critical advantage of the state-space UFIR approach is that, unlike in the Savitsky-Golay and wavelet-based filters, noise reduction and state estimation are provided simultaneously. This presumes higher efficiency in noise reduction and better accuracy in features extraction. Note that the Savitsky-Golay and wavelet-based filters are not state-space estimators. Estimation of higher-order states can be provided using these filters *a posteriori* via the time-derivatives applied to the first state estimate that is typically accompanied with larger noise. As a result, even for the second state, the UFIR smoother produced much more accuracy in the estimation of extreme points of MIT-BIH arrhythmia database.

It worth noticing again that the Savitsky-Golay and wavelet-based filters were already recognized as standard approaches for ECG signals [7], [20]–[29]. In this regard, better performance of the UFIR smoothing algorithm developed in this paper opens new horizons in accurate and precise features extraction from measurements of ECG signals having normal and abnormal heartbeat characteristics.

The UFIR smoother optimized for ECG signals by setting optimal lags and adaptive horizons for each individual degree-polynomial has essentially outperformed the Savitsky-Golay filter, which does not suggest such an optimization [40]–[42]. Accordingly, the following main results were achieved:

1) Optimal denoising and artifacts removal with q_{opt}-lag assigned for each optimal horizon N_{opt}.
2) High accuracy in ECG signal denoising achieved using an adaptive optimal horizon N_{apt}.
3) High accuracy in features extraction achieved taking advantages of the state-space approach.

What left behind is to notice some particular differences between the UFIR and wavelet-based approaches. It has been revealed that errors produced by the wavelet-based filters have a higher dispersion in the extracted features. We explain it by the fact that the available wavelet shapes are not optimal for ECG signals. Furthermore, the wavelet-based filters are not state-space estimators. Therefore, even confusion results can be expected from wavelets. Another specific is that features extracted using the UFIR approach have appeared to be more stable than by the machine learning techniques. That has been demonstrated in a comparison with the EMD, PCA, HT, RR-interval analysis, WT + CNN, and notch filter.

Summarising, we state that the proposed UFIR smoothing approach is more suitable for ECG signals then other techniques and methods considered in this paper. A flaw is the computational time, which is larger than that required by other approaches. Thus, it is still challenging to design fast UFIR smoother-based algorithms, although the computation time of several seconds is not an issue for medical needs.

VIII. CONCLUSION

The state-space UFIR smoothing approach developed in this paper for ECG signal denoising and features extraction has demonstrated better results than methods employing the Savitsky-Golay filter, wavelet-based filtering, and standard filters such as the low-pass, high-pass, notch, and median. That has become possible by designing an adaptive UFIR smoothing algorithm operating with optimal lags on optimal averaging horizons and approximating ECG signals with optimal degree-polynomials. Based upon this algorithm, the extracted features were evaluated by different classifiers and compared to performances provided by other methods. An example of applications given for the P-wave features extraction based on the detected fiducial points, has also shown a potential of the approach in a comparison with the Savitsky-Golay, wavelet-based, and standard filters.

Overall, the adaptive optimized UFIR smoother developed in this paper may open new horizons in efficient denoising and accurate features extraction of ECG signal. Therefore, as future work, we consider further improvement of the algorithm to reduce the computation time and increase the robustness.

REFERENCES

[1] J. Rodrigues, D. Belo, and H. Gamboa, "Noise detection on ECG based on agglomerative clustering of morphological features," *Comput. Biol. Med.*, vol. 87, pp. 322–334, Aug. 2017. doi: 10.1016/j.compbiomed.2017.06.009.
[2] Y. Sun, K. L. Chan, and S. M. Krishnan, "ECG signal conditioning by morphological filtering," *Comput. Biol. Med.*, vol. 32, no. 6, pp. 465–479, Nov. 2002. doi: 10.1016/S0010-4825(02)00034-3.
[3] H. M. Su, T. H. Lin, P. C. Hsu, W. H. Lee, C. Y. Chu, C. S. Lee, W. T. Lai, S. H. Sheu, and W. C. Voon, "Incremental prognostic value of identifying mitral L wave in patients with atrial fibrillation," *Int. J. Cardiol.*, vol. 168, no. 4, pp. 4501–4503, Oct. 2013. doi: 10.1016/j.ijcard.2013.06.118.
[4] L. Smital, M. Vítek, J. Kozumplík, and I. Provazník, "Adaptive wavelet Wiener filtering of ECG signals," *IEEE Trans Biomed. Eng.*, vol. 60, no. 2, pp. 437–445, Feb. 2013. doi: 10.1109/TBME.2012.2228482.
[5] M. S. Manikandan and K. P. Soman, "A novel method for detecting R-peaks in electrocardiogram (ECG) signal," *Biomed. Signal Process. Control*, vol. 7, no. 2, pp. 118–128, Mar. 2012. doi: 10.1016/j.bspc.2011.03.004.
[6] A. Suárez-León, C. Varon, R. Willems, S. Van Huffel, and C. R. Vázquez-Seisdedos, "T-wave end detection using neural networks and Support Vector Machines," *Comput. Biol. Med.*, vol. 96, pp. 116–127, May 2018. doi: 10.1016/j.compbiomed.2018.02.020.
[7] F. Censi, I. Corazza, E. Reggiani, G. Calcagnini, E. Mattei, M. Triventi, and G. Boriani, "P-wave variability and atrial fibrillation," *Nature Publishing Group*, vol. 6, May 2016, Art. no. 26799. doi: 10.1038/srep26799.
[8] R. Alcaraz, F. Hornero, and J. J. Rieta, "Dynamic time warping applied to estimate atrial fibrillation temporal organization from the surface electrocardiogram," *Med. Eng. Phys.*, vol. 35, no. 9, pp. 1341–1348, Sep. 2013. doi: 10.1016/j.medengphy.2013.03.004.
[9] K. Padmavathi and K. S. Ramakrishna, "Classification of ECG signal during atrial fibrillation using autoregressive modeling," *Procedia Comput. Sci.*, vol. 46, pp. 53–59, Jan. 2015.
[10] A. Annavarapu and P. Kora, "ECG-based atrial fibrillation detection using different orderings of conjugate symmetric–complex Hadamard transform," *Int. J. Cardiovascular Acad.*, vol. 2, no. 3, pp. 151–154, Sep. 2016. doi: 10.1016/j.ijcac.2016.08.001.

[11] K. Tateno and L. Glass, "Automatic detection of atrial fibrillation using the coefficient of variation and density histograms of RR and ΔRR intervals," *Med. Biol. Eng. Comput.*, vol. 39, no. 6, pp. 664–671, Nov. 2001. doi: 10.1007/bf02345439.

[12] H. Li, X. Feng, L. Cao, E. Li, H. Liang, and X. Chen, "A new ECG signal classification based on WPD and ApEn feature extraction," *Circuits, Syst., Signal Process.*, vol. 35, no. 1, pp. 339–352, Jan. 2016. doi: 10.1007/s00034-015-0068-7.

[13] H. Li, "Novel ECG Signal Classification based on KICA nonlinear feature extraction," *Circuits, Syst., Signal Process.*, vol. 35, no. 4, pp. 1187–1197, Apr. 2016. doi: 10.1007/s00034-015-0108-3.

[14] H. Li, D. Yuan, X. Ma, D. Cui, and L. Cao, "Genetic algorithm for the optimization of features and neural networks in ECG signals classification," *Sci Rep.*, vol. 7, Jan. 2017, Art. no. 41011. doi: 10.1038/srep41011.

[15] H. Li, X. Wang, L. Chen, and E. Li, "Denoising and R-peak detection of electrocardiogram signal based on EMD and improved approximate envelope," *Circuits, Syst., Signal Process.*, vol. 33, no. 4, pp. 1261–1276, Apr. 2014. doi: 10.1007/s00034-013-9691-3.

[16] H. Li and X. Wang, "Detection of electrocardiogram characteristic points using lifting wavelet transform and Hilbert transform," *Trans. Inst. Meas. Control*, vol. 35, no. 5, pp. 574–582, 2013. doi: 10.1177/0142331212460720.

[17] G. Han and Z. Xu, "Electrocardiogram signal denoising based on a new improved wavelet thresholding," *Rev. Sci. Instrum.*, vol. 87, no. 8, Jul. 2016, Art. no. 084303. doi: 10.1063/1.4960411.

[18] C. Zhan, L. F. Yeung, and Z. Yang, "A wavelet-based adaptive filter for removing ECG interference in EMGdi signals" *J. Electromyogr Kinesiol.*, vol. 20, no. 3, pp. 542–549, Jun. 2010. doi: 10.1016/j.jelekin.2009.07.007.

[19] M. A. Kabir and C. Shahnaz, "Denoising of ECG signals based on noise reduction algorithms in EMD and wavelet domains," *Biomed. Signal Process. Control*, vol. 7, no. 5, pp. 481–489, Sep. 2012. doi: 10.1016/j.bspc.2011.11.003.

[20] K. Kærgaard, S. H. Jensen, and S. Puthusserypady, "A comprehensive performance analysis of EEMD-BLMS and DWT-NN hybrid algorithms for ECG denoising," *Biomed. Signal Process. Control*, vol. 25, no. 11, pp. 178–187, Mar. 2016. doi: 10.1016/j.bspc.2015.11.012.

[21] S. Goel, P. Tomar, and G. Kaur, "An optimal wavelet approach for ECG noise cancellation," *Int. J. Bio-Sci. Bio-Technol.*, vol. 8, no. 4, pp. 39–52, Aug. 2016. doi: 10.14257/ijbsbt.2016.8.4.05.

[22] J. Gao, H. Sultan, J. Hu, and W.-W. Tung, "Denoising nonlinear time series by adaptive filtering and wavelet shrinkage: A comparison," *IEEE Signal Process. Lett.*, vol. 17, no. 3, pp. 237–240, Mar. 2010. doi: 10.1109/LSP.2009.2037773.

[23] S. K. Yadav, R. Sinha, and P. K. Bora, "Electrocardiogram signal denoising using non-local wavelet transform domain filtering," *IET Signal Process.*, vol. 9, no. 1, pp. 88–96, Feb. 2015. doi: 10.1049/iet-spr.2014.0005.

[24] S. Lahmiri, "Comparative study of ECG signal denoising by wavelet thresholding in empirical and variational mode decomposition domains," *Healthcare Technol. Lett.*, vol. 1, no. 3, pp. 104–109, Sep. 2014. doi: 10.1049/htl.2014.0073.

[25] R. N. Vargas and A. C. P. Veiga, "Electrocardiogram signal denoising by clustering and soft thresholding," *IET Signal Process.*, vol. 12, no. 9, pp. 1165–1171, Dec. 2018. doi: 10.1049/iet-spr.2018.5162.

[26] M. García, M. Martínez-Iniesta, J. Ródenas, J. J. Rieta, and R. Alcaraz, "A novel wavelet-based filtering strategy to remove powerline interference from electrocardiograms with atrial fibrillation," *Physiol. Meas.*, vol. 39, no. 11, Nov. 2018. doi: 10.1088/1361-6579/aae8b1.

[27] M. D'Aloia, A. Longo, and M. Rizzi, "Noisy ECG signal analysis for automatic peak detection" *Information*, vol. 10, no. 2, p. 35, Jan. 2019. doi: 10.3390/info10020035.

[28] W. Li, "Wavelets for electrocardiogram: Overview and taxonomy," *IEEE Access*, vol. 7, pp. 25627–25649, 2018. doi: 10.1109/ACCESS.2018.2877793.

[29] R. Chen, Y. Huang, and J. Wu, "Multi-window detection for P-wave in electrocardiograms based on bilateral accumulative area" *Comput. Biol. Med.*, vol. 78, pp. 65–75, Nov. 2016. doi: 10.1016/j.compbiomed.2016.09.012.

[30] R. He, K. Wang, N. Zhao, Y. Liu, Y. Yuan, Q. Li, and H. Zhang, "Automatic detection of atrial fibrillation based on continuous wavelet transform and 2D convolutional neural networks" *Front. Physiol.*, vol. 9, p. 1206, Aug. 2018. doi: 10.3389/fphys.2018.01206.s

[31] J. Lee, B. A. Reyes, D. D. McManus, O. Mathias, and K. H. Chon, "Atrial fibrillation detection using an iPhone 4S," *IEEE Trans. Biomed. Eng.*, vol. 60, no. 1, pp. 203–206, Jan. 2013. doi: 10.1109/TBME.2012.2208112.

[32] U. Maji, M. Mitra, and S. Pal, "Automatic detection of atrial fibrillation using empirical mode decomposition and statistical approach," *Procedia Technol.*, vol. 10, pp. 45–52, Jan. 2013.

[33] P. G. Azbari, "Introducing a combined approach of empirical mode decomposition and PCA methods for maternal and fetal ECG signal processing," *J. Maternal-Fetal Neonatal Med.*, vol. 29, no. 19, pp. 3104–3109, Jan. 2016. doi: 10.3109/14767058.2015.1114089.

[34] R. J. Martis, U. R. Acharya, and L. C. Min, "ECG beat classification using PCA, LDA, ICA and discrete wavelet transform," *Biomed. Signal Process. Control*, vol. 8, no. 5, pp. 437–448, Sep. 2013. doi: 10.1016/j.bspc.2013.01.005.

[35] D. Rezgui and Z. Lachiri, "ECG biometric recognition using SVM-based approach," *IEEJ Trans. Electr. Electr. Eng.*, vol. 11, no. 1, pp. 94–100, Jun. 2016. doi: 10.1002/tee.22241.

[36] M. Sansone, R. Fusco, A. Pepino, and C. Sansone, "Electrocardiogram pattern recognition and analysis based on artificial neural networks and support vector machines: A review," *J. Healthcare Eng.*, vol. 4, no. 4, pp. 465–504, 2013.

[37] A. Savitzky and M. J. E. Golay, "Smoothing and differentiation of data by simplified least squares procedures," *Anal. Chem.*, vol. 36, no. 8, pp. 1627–1639, 1964. doi: 10.1021/ac60214a047.

[38] S. Hargittai, "Savitzky–Golay least-squares polynomial filters in ECG signal processing" in *Proc. Comput. Cardiol.*, Sep. 2005, pp. 763–766.

[39] I. Dotsinsky and G. S. Mihov, "Tremor suppression in ECG," *Biomed. eng. online*, vol. 7, p. 29, Nov. 2008. doi: 10.1186/1475-925X-7-29.

[40] S. R. Krishnan and C. S. Seelamantula, "On the selection of optimum Savitzky-Golay filters," *IEEE Trans. Signal Process.*, vol. 61, no. 2, pp. 380–391, Jan. 201. doi: 10.1109/TSP.2012.2225055.

[41] Y. Hong and Y. Lian, "A memristor-based continuous-time digital FIR filter for biomedical signal processing," *IEEE Trans. Circuits Syst. I, Reg. Papers*, vol. 62, no. 5, pp. 1392–1401, May 2015. doi: 10.1109/TCSI.2015.2403033.

[42] R. Sameni, "Online filtering using piecewise smoothness priors: Application to normal and abnormal electrocardiogram denoising," *Signal Process.*, vol. 133, pp. 52–63, Apr. 2016. doi: 10.1016/j.sigpro.2016.10.019.

[43] Y. S. Shmaliy and L. J. Morales-Mendoza, "FIR smoothing of discrete-time polynomial signals in state space," *IEEE Trans. Signal Process.*, vol. 58, no. 5, pp. 2544–2555, May 2010. doi: 10.1109/TSP.2010.2041595.

[44] Y. S. Shmaliy and O. Ibarra-Manzano, "Optimal and unbiased FIR filtering in discrete time state space with smoothing and predictive properties," *EURASIP J. Adv. Signal Process.*, vol. 2012, p. 163, Dec. 2012. doi: 10.1186/1687-6180-2012-163.

[45] Y. S. Shmaliy, O. Ibarra-Manzano, L. Arceo-Miquel, and J. Munoz-Diaz, "A thinning algorithm for GPS-based unbiased FIR estimation of a clock TIE model," *Measurement*, vol. 41, no. 5, pp. 538–550, Jun. 2008. doi: 10.1016/j.measurement.2007.05.001.

[46] S. Zhao, Y. S. Shmaliy, and F. Liu, "Fast Kalman-like optimal unbiased FIR filtering with applications," *IEEE Trans. Signal Process.*, vol. 64, no. 9, pp. 2284–2297, May 2016. doi: 10.1109/TSP.2016.2516960.

[47] S. Zhao and Y. S. Shmaliy, "Unified maximum likelihood form for bias constrained FIR filters," *IEEE Signal Process. Lett.*, vol. 23, no. 12, pp. 1848–1852, Dec. 2016.

[48] Y. S. Shmaliy, S. Zhao, and C. K. Ahn, "Unbiased finite impluse response filtering: An iterative alternative to Kalman filtering ignoring noise and initial conditions," *IEEE Control Syst. Mag.*, vol. 37, pp. 70–89, Oct. 2017.

[49] C. Lastre-Domínguez, Y. S. Shmaliy, O. Ibarra-Manzano, and L. J. Morales-Mendoza, "Unbiased FIR denoising of ECG signals," in *Proc. 14th Int. Conf. Elect. Eng., Comput. Sci. Autom. Control (CCE)*, Sep. 2017, pp. 1–6.

[50] C. Lastre-Domínguez, Y. S. Shmaliy, O. Ibarra-Manzano, J. Munoz-Minjares, and L. J. Morales-Mendoza, "ECG signal denoising and features extraction using unbiased FIR smoothing," *Biomed Res. Int.*, vol. 2019, Feb. 2019, Art. no. 2608547. doi: 10.1155/2019/2608547.

[51] A. L. Goldberger, "PhysioBank, physiotoolkit, and physiobank, physiotoolkit, and physionet: Components of a new research resource for complex physiologic signals" *Circulation*, vol. 101, no. 23, pp. 215–220, Jun. 2000. doi: 10.1161/01.CIR.101.23.e215.

[52] P. W. Macfarlane, *Comprehensive Electrocardiology*. London, U.K.: Springer, 2010.

[53] A. L. Goldberger, *Goldberger's Clinical Electrocardiography—A Simplified Approach*, 8th ed. Pennsylvania, PA, USA: Elsevier, 2013.

[54] Y. S. Shmaliy, "An unbiased FIR filter for TIE model of a local clock in applications to GPS-based timekeeping," *IEEE Trans. Ultrason., Ferroelectr., Freq. Control*, vol. 53, no. 5, pp. 862–869, May 2006. doi: 10.1109/TUFFC.2006.1632677.
[55] F. Ramirez-Echeverria, A. Sarr, and Y. S. Shmaliy, "Optimal memory for discrete-time FIR filters in state-space," *IEEE Trans. Signal Process.*, vol. 62, no. 3, pp. 557–561, Feb. 2014. doi: 10.1109/TSP.2013.2290504.
[56] J. Pan and W. J. Tompkins, "A real-time QRS detection algorithm," *IEEE Trans. Biomed. Eng.*, vol. BME-32, no. 3, pp. 230–236, Mar. 1985. doi: 10.1109/TBME.1985.325532.
[57] I. Beraza and I. Romero, "Comparative study of algorithms for ECG segmentation," *Biomed. Signal Process. Control*, vol. 34, pp. 166–173, Apr. 2017. doi: 10.1016/j.bspc.2017.01.013.
[58] E. J. D. S. Luz, D. Menotti, and W. R. Schwartz, "Evaluating the use of ECG signal in low frequencies as a biometry," *Expert Syst. Appl.*, vol. 41, no. 5, pp. 2309–2315, 2014. doi: 10.1016/j.eswa.2013.09.028.
[59] J. Aspuru, A. Ochoa-Brust, R. A. Félix, W. Mata-López, L. J. Mena, R. Ostos, and R. Martínez-Peláez, "Segmentation of the ECG Signal by means of a linear regression algorithm," *Sensors*, vol. 19, no. 4, p. 775, Feb. 201. doi: 10.3390/s19040775.
[60] B. N. Singh and A. K. Tiwari, "Optimal selection of wavelet basis function applied to ECG signal denoising," *Digit. Signal Process.*, vol. 16, no. 3, pp. 275–287, May 2006. doi: 10.1016/j.dsp.2005.12.003.
[61] J. Y. A. Foo, "Comparison of wavelet transformation and adaptive filtering in restoring artefact-induced time-related measurement," *Biomed. Signal Process. Control*, vol. 1, no. 1, pp. 93–98, 2006. doi: 10.1016/j.bspc.2017.01.013.
[62] Z. Zidelmal, A. Amirou, M. Adnane, and A. Belouchrani, "QRS detection based on wavelet coefficients," *Comput. Methods Programs Biomed.*, vol. 107, no. 3, pp. 490–496, Sep. 2012. doi: 10.1016/j.cmpb.2011.12.004.
[63] R. J. Martis, U. R. Acharya, and H. Adeli, "Current methods in electrocardiogram characterization," *Comput. Biol. Med.*, vol. 48, pp. 133–149, May 2014. doi: 10.1016/j.compbiomed.2014.02.012.
[64] E. J. da S. Luz, W. R. Schwartz, G. Cámara-Chávez, and D. Menotti, "ECG-based heartbeat classification for arrhythmia detection: A survey," *Comput. Methods Programs Biomed.*, vol. 127, pp. 144–164, Apr. 2016. doi: 10.1016/j.cmpb.2015.12.008.

CARLOS LASTRE-DOMÍNGUEZ (M'17) was born in Sinc, Colombia, in 1987. He received the B.S. degree from the Universidad de Pamplona, Colombia, in 2011, and the M.I. degree from the Universidad Industrial de Santander, Santander, Colombia, in 2016. He is currently pursuing the Ph.D. degree in electrical engineering with the Universidad de Guanajuato. His scientific research interests include machine learning, digital signal processing, and optimum filter applied to biomedical signals. He has also participated in various congresses on these topics.

YURIY S. SHMALIY (M'96–SM'00–F'11) received the B.S., M.S., and Ph.D. degrees from the Kharkiv Aviation Institute, Ukraine, in 1974, 1976, and 1982, respectively, all in electrical engineering, and the D.Sc. degree from the Kharkiv Railroad Institute, in 1992. He was a Full Professor, in 1986. From 1985 to 1999, he was with Kharkiv Military University. In 1992, he founded the Scientific Center Sichron, where he was the Director, in 2002. From 2015 to 2016, he was a Visiting Researcher with the City, University of London, and in 2015 and from 2017 to 2019, he was with Telecom SudParis. Since 1999, he has been with the Universidad de Guanajuato, Mexico, where he was the Head of the Department of Electronics Engineering, from 2012 to 2015. He has published more than 450 journals and conference papers and holds 81 patents. His books are *Continuous-Time Signals* (Springer, 2006), *Continuous-Time Systems* (Springer, 2007), and *GPS-Based Optimal FIR Filtering of Clock Models* (New York: Nova Science Publishers, 2009). He also edited a book *Probability: Interpretation, Theory and Applications* (New York: Nova Science Publishers, 2012) and contributed to several books with invited chapters. His discrete orthogonal polynomials are called Shmaliy moments. His current research interests include optimal estimation, statistical signal processing, and stochastic system theory. He was rewarded a title Honorary Radio Engineer of the USSR, in 1991. He was listed in the Outstanding People of the 20th Century, Cambridge, U.K., in 1999, and has received the Royal Academy of Engineering Newton Research Collaboration Program Award, in 2015. He is currently an Associate Editor and an Editorial Board Member in several journals. He was invited many times to give tutorial, seminar, and plenary lectures.

OSCAR IBARRA-MANZANO (M'00) was born in Mexico, in 1968. He received the B.S. degree in communications and electronics and the M.E. degree in electrical engineering from the Universidad de Guanajuato, Salamanca, in 1990 and 1993, respectively, and the Ph.D. degree in electrical engineering from the National Institute for Astrophysics Optics and Electronics, Puebla, Mexico, in 1999. He was the Dean of the Mechanical, Electrical and Electronics Engineering School, from 2003 to 2012. In 1991, he joined the Universidad de Guanajuato, where he has been a Full-Time Professor and the Chair of the Electronics Engineering Department, since 2000.

MIGUEL VAZQUEZ-OLGUIN (M'16) was born in Mexico, in 1982. He received the B.S. degree in electronics and communications from the Universidad Iberoamericana de Len, Len, Mexico, in 2005, and the M.S. degree in electronics and communications from the Center for Scientific Research and Higher Education of Ensenada, Ensenada, Mexico, in 2009. He is currently pursuing the Ph.D. degree with the Universidad de Guanajuato, Salamanca, Mexico. His current research interests include consensus filtering, wireless sensor networks, and optimal estimation.